Terahertz local oscillator for the Microwave Limb Sounder on the Aura satellite

Eric R. Mueller,[1] Robert Henschke,[1] William E. Robotham, Jr.,[1] Leon A. Newman,[1] Lanny M. Laughman,[1] Richard A. Hart,[1] John Kennedy,[1] and Herbert M. Pickett[2,*]

[1]Coherent Inc., 1280 Blue Hills Avenue, Bloomfield, Connecticut 06002, USA
[2]Jet Propulsion Laboratory, California Institute of Technology, Pasadena, California 91109, USA

*Corresponding author: herbert.m.pickett@jpl.nasa.gov

Received 12 January 2007; accepted 30 March 2007;
posted 6 April 2007 (Doc. ID 78807); published 3 July 2007

The Microwave Limb Sounder on the Aura satellite has a radiometer at 2.5 THz to perform global mapping of OH in the atmosphere. The OH radiometer utilizes two Schottky-diode mixers pumped by an optically pumped THz gas laser local oscillator. The laser was first turned on in space on July 22, 2004, and has performed without issue for more than 30 months. The specifications, design, and modeling of this 2.5 THz laser local oscillator are presented here, along with some of the important design validation and test results. © 2007 Optical Society of America

OCIS codes: 140.4130, 140.3470, 140.3070, 030.5630.

1. Introduction

The Microwave Limb Sounder (MLS) on the Aura satellite has a radiometer at 2.5 THz to perform a global mapping of OH in the atmosphere. The OH radiometer utilizes two Schottky-diode mixers [1] pumped by an optically pumped THz gas laser local oscillator (GLLO). Readers are referred to a description of the GLLO preliminary design [2], an overall description of the MLS instrument [3], and a more detailed description of the THz radiometer [4]. The GLLO was designed, fabricated, and delivered by Coherent, Inc. The THz radiometer is one of five heterodyne radiometer channels on the MLS. While Coherent provided the GLLO for the THz radiometer, Jet Propulsion Laboratory (JPL) fabricated the receivers, performed the system integration, monitored the instrument operation, and performed the atmospheric data retrieval. The GLLO program included a demonstration program, an Engineering Model (EM), and a Flight Model (FM). The EM and FM had the same electrical and mechanical interfaces, but the EM contained lower reliability parts and had reduced testing requirements.

0003-6935/07/224907-09$15.00/0

While many readers may have experience with moderate-to-low reliability optically pumped far-infrared (THz) lasers, high-reliability THz lasers may not be familiar. Starting with the pump laser technology: the GLLO utilizes the same high-reliability, sealed-off, rf-excited, CO_2 laser technology found in Coherent's commercial lasers and in numerous high-sophistication systems Coherent has delivered over the years. Specifically, this technology has demonstrated: operating life in excess of 40,000 h, shelf life of more than 15 years, operation in high-performance aircraft environments, spectral purity and stability sufficient for coherent lidar applications, and all within a very compact and rugged package.

Applicable vacuum and optical techniques from the CO_2 laser design are incorporated into the THz laser design. Thus while Coherent staff have constructed ultrahigh-stability and spectral purity THz lasers that have operated for years with only periodic gas refills, the sealing and mirror mount technologies adopted from the CO_2 laser designs yielded THz lasers that operate for years without refilling or service of any kind.

In the design of a system as intricate, efficient, and autonomous as the GLLO, a number of complex interactions, which may not be imperative for a laboratory-

based system, must be considered to assure a robust design. The remainder of this paper will present the GLLO design, with limited details, in the sections that follow: GLLO Specifications, GLLO Configuration, High-Efficiency Pump Laser, Pump Laser Frequency Control, THz Laser, On-orbit Performance, and Conclusions.

It should be pointed out that Coherent was merely the leader of the GLLO team. The other team members were: Aerospace Structural Research (mechanical/thermal design and analysis), Teledyne Brown Engineering, Group Technologies (electronics fabrication), and JPL (general system design guidance). The team also relied on a network of vital suppliers too numerous to mention.

2. GLLO Specifications

The GLLO has a long list of specifications. In the interest of brevity only those specifications which relate to topics covered in this paper will be presented.

The GLLO must autonomously operate and produce sufficient output power to optimize two Schottky-diode receivers. The output power specification is 18 mW. The required lifetime is five years on orbit plus 2200 h of ground testing. All specifications are required to be met over the entire lifetime of the GLLO and thus constitute the definition of lifetime.

There are significant constraints on available prime power, mass, and envelope. The entire GLLO (including all control electronics) must fit in a box no larger than $75 \times 30 \times 10$ cm. The allowed total mass is <22 kg, and the total available 28 V dc prime power is 120 W. The size/mass/efficiency portion of the specification drives a large part of the GLLO design.

Further mechanical constraints are in force via the launch survival specification. While the GLLO does not have to operate during launch, it must of course survive launch. With the GLLO's position on the Delta II launch vehicle, this amounts to 15.8 G rms for 1 min on all three axes. Further, with the launch platform's acceleration profile, the time from atmospheric pressure to 1 Torr is $\sim$20 s. Therefore adequate venting must be provided to prevent rupture of nonpressure enclosures.

The frequency stability requirement is 100 kHz/s full width at half maximum, long-term drift not to exceed 2 MHz from line-center, and spectral purity sidebands <-30 dBc ($>$200 kHz off carrier). Since a Super Invar structure would not be compatible with the mass budget, Coherent devised a novel method of active frequency control for the THz laser.

The required amplitude stability is 1% over 30 s. System level Rigrod modeling [5] has shown this to be dominated by feedback interaction with the diplexer/receiver system. Coherent devised a novel method to mitigate this effect as well.

The output spatial mode specification is that only power in the specified Gaussian TEM00 mode is counted, and the GLLO output beam waist must be 4.1 mm located 465 mm from the GLLO-radiator interface.

The output polarization specification is equal parts horizontal and vertical (within 10%) with any phase relationship. Thus circular polarization or 45° linear polarization is acceptable, and 45° linear was selected as the baseline for the GLLO.

All of the performance specifications must be met in the presence of feedback from the diplexer/receivers. This is expected to be less than 20%. Accordingly, the specification is robustness to up to 20% THz feedback of arbitrary phase and polarization. Coherent has devised a method to mitigate the THz feedback, as will be presented in the THz laser section. The temperature range specification for the GLLO is nontrivial as well. The system will be tested from -10 °C to 50 °C (operational), and from -35 °C to 60 °C (non-operational survival).

3. GLLO Configuration

The GLLO block diagram is shown in Fig. 1. The GLLO electronically interfaces with the MLS via three main connections: prime power, RS-422 communications, and mixer bias signal.

To illustrate the operation of the GLLO, "follow the power." Prime power is converted into rf power in the rf power supply. The rf power propagates through coaxial semi-rigid to the pump laser and excites the pump laser. The emitted 9.69 μm light propagates through the pump beam delivery optics and into the THz laser. The THz laser converts the pump light to THz light at 118.83 μm (2.52 THz). Finally the THz beam delivery optics transform the laser output mode to match the specified output profile.

The pump beam delivery optics include a lens that focuses the beam into the THz laser. Using crossed Brewster pairs to "pick off" small portions of the pump beam, beam samples are sent to the pyroelectric detector (which is used by the pump laser frequency/amplitude control electronics), and to the thermopile (pump power, health, and status). A near-Brewster wedge is utilized to provide 500 mW of pump radiation to the photoacoustic cell.

The output from the THz laser is transformed to match the specified beam profile via a Newtonian telescope. This telescope is formed by an off-axis hyperbola, and an off-axis elliptical mirror. The fastest/f number in the telescope is $\sim$7. The mirrors are

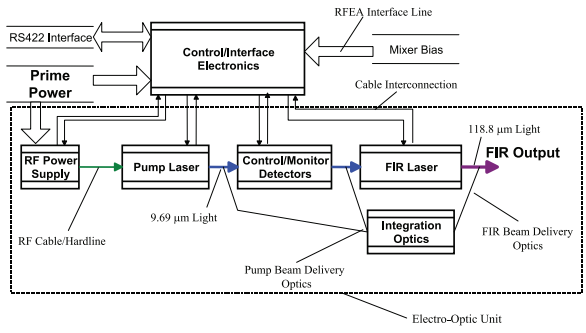

Fig. 1. (Color online) Block diagram of GLLO.

diamond-turned Al, fabricated as part of their respective optical mounts.

The THz shutter is included to prevent a gain-switched THz spike, possible during initial turn-on, from damaging the receivers. (Note that if conditions are right, the pump laser can put out a ~500 W pulse at turn-on.) The back of the shutter is mirrored, so that when the shutter is closed the THz beam will propagate into the THz thermopile (health and status). As the output telescope for the THz beam is Newtonian, the focal spot from the telescope is an ideal location for coupling into the thermopile. This obviates the need for any additional THz focusing element.

The GLLO's mechanical interface with the MLS is through three bipod struts that mount the GLLO to the THz module. A radiator plate is mounted to the GLLO optical baseplate and radiates the waste heat created by the GLLO. The radiator is not structural; in fact, the GLLO provides the support for the radiator.

4. High-Efficiency Pump Laser

The first requirement for a high-efficiency pump laser is a high-efficiency rf power supply. In the demonstration program, Coherent demonstrated 75 W of rf out with 100 W of dc in. For the EM and FM, Coherent reallocated power within the GLLO, providing 110 W of dc power to the rf power supply. With this level of input power, 85 W of rf has been demonstrated. Thus the pump laser had 85 W of rf pump. Effective use of the available rf power is also key to high-efficiency operation. Through a number of patented techniques, Coherent was able to couple the rf power efficiently into the discharge. The rf power supply is a conductively cooled device that uses a class-C power amplifier stage.

Diagrams of the high-efficiency pump laser are shown in Fig. 2. This laser is very compact and low in mass (1.5 kg). The rf circuit of the laser is formed by the combination of the electrode/waveguide/enclosure capacitance and the resonating inductors. The rf power is admitted through an rf feedthrough in the side of the laser. The cavity is formed by the output coupler, on one end, and the high-efficiency line selector, on the other. This line selector greatly increases the efficiency of the laser, as it has an effective reflectivity at 9P36 of >99%.

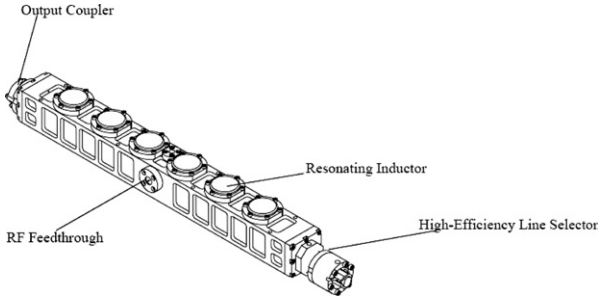

Fig. 2. High-efficiency pump laser.

As with the entire GLLO project, extensive mathematical modeling of the pump laser has been utilized. In particular, Coherent has measured Rigrod parameters for a complete distributed-loss Rigrod model [5] of the pump laser.

In the demonstration program, Coherent delivered an integrated pump laser/RFPS that had an output power of >9 W at 9P36 with 100 W of dc input. This laser also exhibited single-mode operation, a property Coherent has found to be important for highest-efficiency THz operation. It should be noted that, because of time and available optics constraints, the cavity optics in the delivered demonstration laser were not optimal. Based on the Rigrod model for the pump laser, with an optimized cavity Coherent obtained 11 W out in the FM laser with 85 W of rf in.

The FM laser has several capabilities to facilitate reliable ignition in space. Before ignition, the rf impedance and resonant frequency of the laser are substantially different than after ignition. Accordingly, the rf power supply can be set to a different frequency to match the laser rf resonance or a relay can be selected to change the matching network for the laser cavity. After very long times of inactivity (months) at temperatures <5 °C, the pump laser could be difficult to ignite even with these two techniques. To facilitate ignition, the GLLO can be preheated with a relay-activated 60 W heater if the starting temperature is too low. The heater is automatically turned off before pump laser ignition so that total dc power never exceeds the allowed allocation.

5. Pump Laser Frequency Control

Precise control of the pump frequency is essential for the GLLO to meet all specifications. During the demonstration program the effects of operating the pump laser at its line-center were studied, as this could significantly simplify the frequency control. However, it was found that operation at 9P36 line-center causes a 2 dB loss in THz efficiency. Therefore it was decided that this would not be acceptable.

Another possible frequency control scheme would involve trying to lock the pump frequency by observing the THz output. Careful analysis and modeling showed this to be a poor approach, entangling numerous physical effects and making the frequency control nonrobust at best.

To obtain an absolute frequency reference to lock the laser against, a photoacoustic cell (see Fig. 3), which uses the THz laser vibrational pump transition in methanol [6], was designed and tested.

The PA cell is a very simple device. Essentially it is a sealed cavity that contains methanol at ~2.2 Torr, a prepolarized microphone, and AR windows.

The physical basis for the PA cell-based pump frequency locking method is presented in Fig. 4. The pump laser is dithered about the center of the methanol absorption peak, producing an acoustic signal as the amount of absorbed power is modulated.

The pump laser frequency modulation will couple into the THz output spectrum through two sources. The first of these, Doppler coupling induced by veloc-

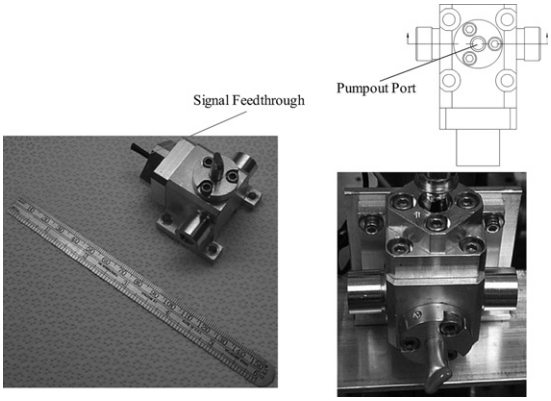

Fig. 3. Photoacoustic molecular frequency standard.

ity memory effects, is given, in worst case, by

$$\mathrm{FM}_{\mathrm{THz}} = \mathrm{FM}_{\mathrm{pump}} \frac{\nu_{\mathrm{THz}}}{\nu_{\mathrm{pump}}}, \tag{1}$$

where $\mathrm{FM}_{\mathrm{THz}}$ is the Doppler-coupling-induced THz frequency modulation, $\mathrm{FM}_{\mathrm{pump}}$ is the FM dither impressed on the pump laser, THz is the THz operating frequency, and ν_{pump} is the pump frequency. With the parameters for the GLLO's THz laser, the Doppler-coupling factor is $\sim 1/12$. Therefore the induced THz dither will be down by a factor of 12 with respect to the pump dither. As Coherent demonstrated this lock with <1 MHz of pump dither, this was confirmed to be acceptable with respect to the 100 kHz short-term frequency noise specification.

The above does not exhaust sources of frequency noise induced by this locking technique. There is an effect known as the two-photon-light-shift (TPLS), for standing-wave THz lasers [7,8]. This is a high-frequency, Autler-Townes [9] Stark effect, where the Stark field is the pump field. A number of papers on this effect have been published. The GLLO team has used the results in these papers to construct a model of the TPLS. While this model is not complete, it does give good agreement with the measured results for other THz lines. There do not appear to be any direct measurements of the TPLS for the 2.52 THz line but other authors [10] have indicated that the TPLS appears to be anomalously small for this transition.

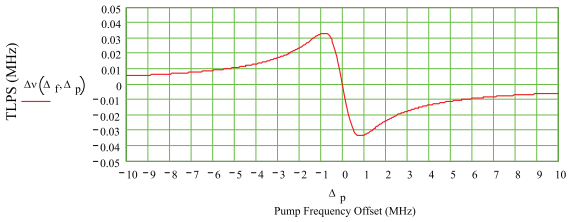

Fig. 5. Two-photon light shift versus pump offset.

The general form of the TPLS effect is given by [7,8]

$$\Delta\nu_{\mathrm{THz}} = \frac{\left[-\Delta_f - \dfrac{\beta^2\Delta_p}{2\Delta_p{}^2 + \gamma^2/8}\right]}{1 + 2\pi\dfrac{\gamma}{c\alpha}}, \tag{2}$$

where Δ_f is the THz cavity offset from THz line-center, γ is the vibrational and rotational (assumed same) homogenous linewidth, Δ_p is the pump laser frequency offset from the vibrational transition (in methanol) line-center, β is the Rabi frequency for the pump transition, α is the THz gain per unit length, and the factor in the denominator is the THz gain-reduced pulling factor. It should be noted that β is in general proportional to the pump field magnitude (which is proportional to the square root of pump field density), and $\Delta\nu_{\mathrm{THz}}$ is proportional to pump power density.

As there is noticeable uncertainty in published values for the dipole matrix element [8,11], and considerable inaccuracy in estimating the circulating pump intensity [12], we estimated β from combining a model for a circulating pump field [13] with data obtained during the demonstration program.

The results of the TPLS modeling are presented in Figs. 5 and 6. As shown there the expected TPLS is 60 kHz, with the worst case at 1 MHz of pump dither, and the TPLS can be minimized by operating the pump laser only slightly off the methanol line-center. Further, as indicated earlier, an anomalously small TPLS has been reported for the 2.52 kHz laser transition. This modeling projection was validated by measurements of GLLO output spectral purity made during acceptance tests to be described next.

It should be noted that the line selector end of the pump laser also contains a piezoelectric translator (PZT) that maximizes its reflectivity. This length is

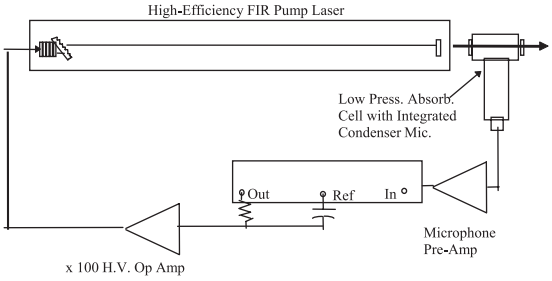

Fig. 4. Pump-laser frequency locking method.

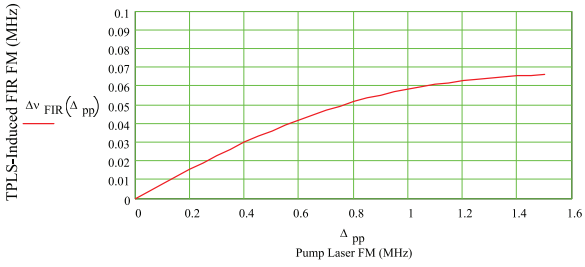

Fig. 6. Worst-case two-photon light shift versus pump dither.

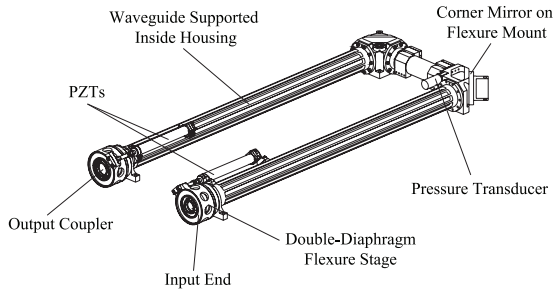

Fig. 7. Standing-wave THz laser.

dither stabilized for maximum pump laser power. Modeling of the effect of this dither shows that it has negligible effect on the pump frequency (60:1 ratio of effective frequency modulation). Thus, there are two dither control loops, operating at different frequencies, which control the frequency and output power of the laser.

6. THz Laser

For reasons of risk [14] and schedule, the option of a ring THz laser was dropped from the GLLO early in the program. A drawing of the standing-wave THz laser for the GLLO is shown in Fig. 7.

Both the input and output mirrors are mounted on PZT-actuated flexure stages. The corner mirrors are mounted on diaphragm flexure alignment mounts. The housing is aluminum with the fused quartz dielectric waveguides supported inside with flexible wavesprings.

The input coupler and turn mirrors are diamond-turned copper. The input coupling is through a hole in the input mirror. The output coupler is a uniform capacitive mesh-type coupler [15], fabricated by the University of Massachusetts Lowell, STL and POD laboratories. Design of the mesh output couplers was accomplished using the GLAYERS program of CSIRO.

Both the THz modeling and the demonstration program results showed optimal uniform output coupling to be necessary to achieve high-efficiency operation. Some of the output power versus pump power results obtained during the demonstration program

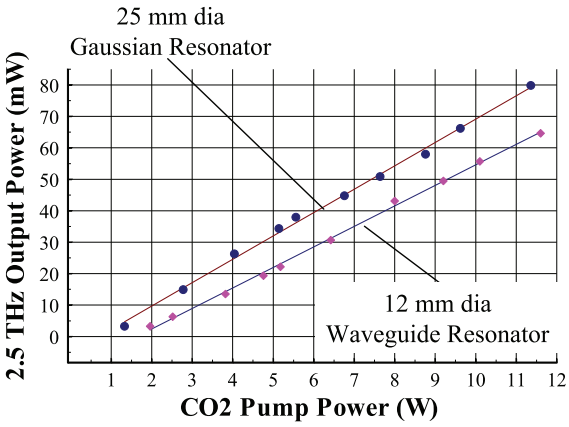

Fig. 8. 1.5 m straight-guide demonstration program THz results.

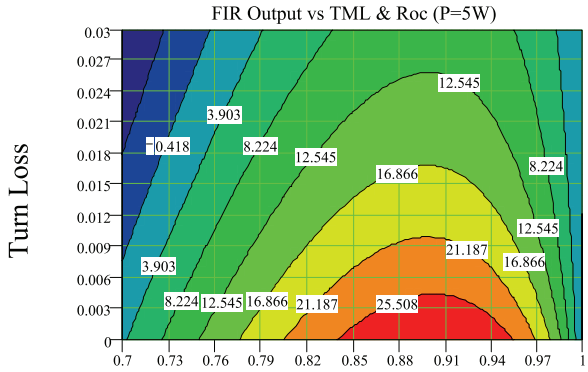

Fig. 9. Rigrod prediction for THz output versus turn loss and output coupling.

are presented in Fig. 8. All of those data were obtained with the pressure held fixed at the optimal pressure for 5 W of pump power, to more accurately simulate flight conditions (i.e., once sealed, the THz pressure cannot be adjusted and optimization for the low end of pump power is prudent). The results in Fig. 8 bracket the cavity geometries required to meet the initial internal goal of 20 mW out with 5 W of pump power. In looking at Fig. 8, it should be remembered that the delivered pump laser actually had an output power of >9 W. Thus, a great deal of margin was demonstrated.

The results of Fig. 8 are for a straight-guide laser and the losses associated with cavity turns are expected to reduce efficiency and improve mode selection. Coherent developed a distributed-loss Rigrod model for the THz laser. The results of this model with 5 W of pump are summarized in Figs. 9 and 10.

Figure 9 plots the output power versus output coupling and turn loss, with pump power fixed at 5 W. Figure 10 presents the output power versus turn loss with the output coupling fixed at 9%, and the pump power fixed at 5 W. All of the parameters for the Rigrod model were determined experimentally during the demonstration program. There were no adjustable parameters at this stage of the modeling effort. The most important conclusion of these figures is that turn loss is the key to high-efficiency operation. The GLLO's THz laser operates in the low-gain low-loss regime; thus, any loss is significant. Although not shown in this paper, the experimental

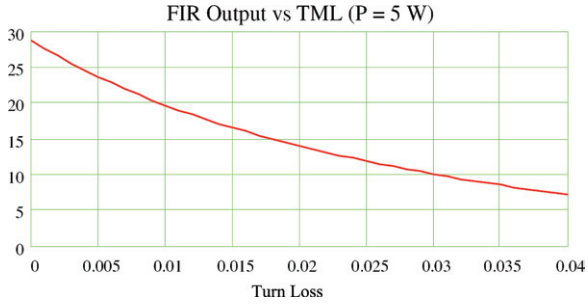

Fig. 10. Rigrod prediction for THz output versus turn loss. Output coupling fixed at 9%, pump power fixed at 5 W.

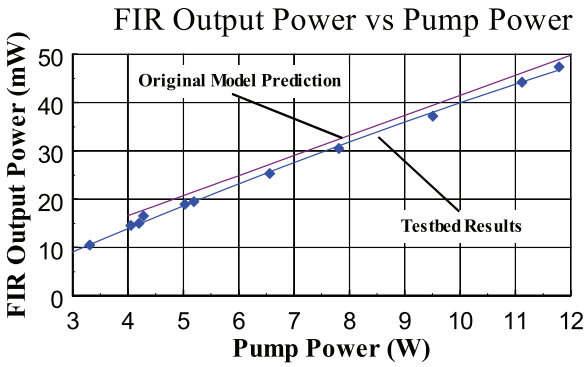

Fig. 11. Test-bed results: comparison with original model.

results for a folded THz laser show the threshold regime to be below 5 W of pump power. Thus, the GLLO's THz laser will not be operating in the threshold regime.

The dependence of the GLLO output power on pump power is shown in Fig. 11. The predicted performance from the Rigrod model is in excellent agreement with the observed output power for the test-bed laser. This result gave confidence that the performance of the EM and FM lasers would perform as predicted by the model.

7. Output Frequency and Amplitude Control

The issue of THz feedback from the diplexer/receivers, combined with the schedule and performance risks associated with a ring laser, directed the GLLO program toward a novel method for feedback mitigation. Fig. 12 illustrates the basis for the approach.

The feedback can be considered as a part of the THz output coupler. This is effectively an etalon output coupler whose reflectivity and effective phase shift are given by

$$E_r(L_{cc},\ R_{oc},\ R_{fb}) = \sqrt{R_{oc}}' - \frac{e^{-4\pi i L_{cc}/\lambda}(1-R_{oc})\sqrt{R_{fb}}}{1-e^{-4\pi i L_{cc}/\lambda}\sqrt{R_{oc}R_{fb}}}, \quad (3)$$

$$\phi = \arg(R_r), \quad (4)$$

where E_r is the reflected complex E field seen at the output coupler, L_{cc} is the "coupled-cavity" length, R_{oc} is the reflectivity of the output coupler, R_{fb} is the feedback reflectivity, λ is the THz wavelength, and ϕ is the effective phase seen at the output coupler.

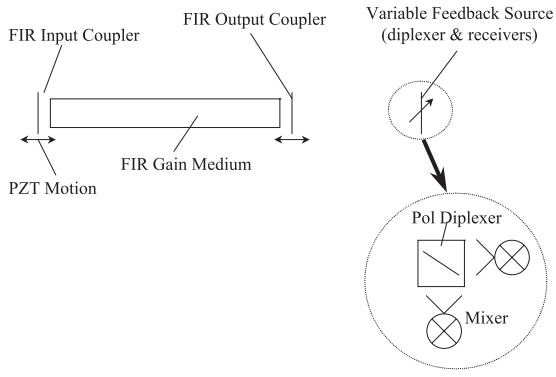

Fig. 12. THz feedback mitigation approach.

A signal from one of the mixer bias lines is fed into the GLLO control electronics and used to optimize the output power at all times. Since the GLLO control electronics have the ability to command both cavity end mirrors, and the pump laser is locked to an absolute reference, the THz frequency can be assured to be at line-center.

Effects of this control strategy have been modeled and are presented in Fig. 13. Figure 13(a) shows the frequency pulling as a function of change in feedback percentage and coupled-cavity length. (Δl is the change in distance between the diplexer/receivers and the THz output coupler.) Figure 13(b) shows the effective reflectivity versus Δl and feedback percentage. Figure 13(c) shows the THz output power vs Δl and turn loss at a fixed pump power of 5 W. These figures demonstrate that

- THz feedback results in both frequency and amplitude pulling,
- reflectivity pulling drives the efficiency, and
- the magnitude of the effects increases rapidly with increasing feedback percentage.

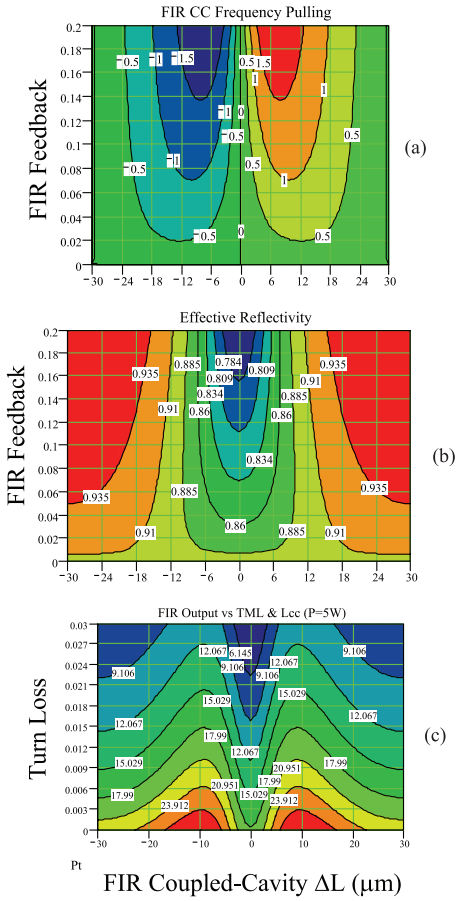

Fig. 13. THz feedback control effects. (a) THz frequency pulling [MHz] versus THz feedback and change in "coupled-cavity" length (Δl), (b) effective output coupling versus THz feedback Δl, and (c) predicted THz output versus turn loss and Δl, pump fixed at 5 W.

Further analysis also reveals that the THz feedback acts most strongly in amplitude and second in frequency. Accordingly, the GLLO output power is optimized by performing a three-point maximization of both the THz input coupler and the THz output coupler. The output power measurement comes from the mixer bias when the shutter is open and comes from the THz thermopile when the shutter is closed. The duration of the steps is adjusted for the response of these two detectors. The step size taken for the three-point optimizations is 8 MHz and corresponds to the half-power point for the GLLO output power. This step size is larger than the ripple in output power observed with a period of 5 μm because of standing waves from the pump laser. The time for the optimization is signaled by a command issued by the MLS control computers so that the optimization can take place when the THz scan mechanism is retracing and no useful data is being taken. The maximum time between optimizations is currently 247 s, although optimization is done as soon as 24.7 s if the GLLO output power has deteriorated.

8. Acquisition and Control Software

The GLLO is controlled by a radiation-hard version of an 8051 processor with 64 kbytes of memory. The controller responds to commands from the MLS computers via an RS-422 serial interface at 9600 baud. A total of 31 commands allow GLLO turn-on, acquisition, and control, as well as testing, status, and monitoring of key voltages and temperatures. If necessary, the entire code for the GLLO stored in EEPROM can be loaded from the ground.

For a near-polar-orbit satellite, the opportunities for commanding the satellite are limited, and it is essential that the GLLO operate nearly autonomously. The GLLO software must optimize the output power and jump modes if the four piezotranslators reach the end of their travel. Power optimization or reacquisition is synchronized with the MLS instrument scan cycle (24.6 s) with a command from the MLS onboard control processor. On receipt of the command, the GLLO software takes action to relock and optimize the laser. A second automatic command sent from the MLS control processor at 0.167 s intervals provides telemetry for 16 GLLO sensors and voltages. In 26 months of on-orbit operation, the GLLO has not needed any ground intervention except for two or three incidences when power was cycled. Achieving nominal GLLO operation after power on requires two ground-initiated commands.

9. Acceptance Tests and On-Orbit Performance

The GLLO FM unit underwent a number of tests including vibration tests, thermal vacuum tests, and rf-interference tests. These tests were repeated as part of the instrument testing and again as part of spacecraft testing. In addition, there were several acceptance tests made only at Coherent that verified GLLO specifications.

Figure 14 shows the output profile of the GLLO. This profile was measured at several positions to estimate the radius of curvature of the phase front. The position of the beam waist called out in the specifications was established with an alignment template that was also used to align the rest of the THz radiometer at JPL. At the specified beam waist, a 2D fit of the profile gave $w_H = 4.13$ mm and $w_V = 4.13$ mm, compared with the specified $w = 4.1$ mm. The alignment of the observed and specified centers was better than 0.14 mm, and the focus mismatch was 0.8%. The total mode match was >93%, and the polarization was 39°.

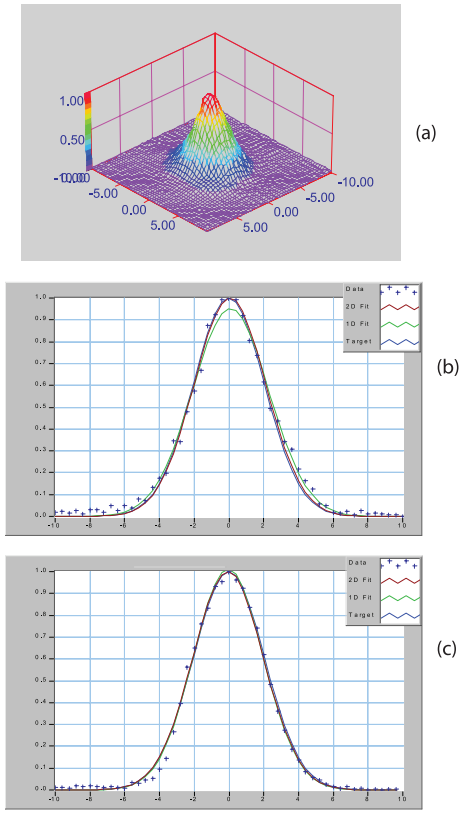

Fig. 14. GLLO output beam profile: (a) 2D profile, (b) horizontal cross-section, and (c) vertical cross-section.

Spectral purity was checked by combining a portion of the GLLO output with a second THz laser in a waveguide mixer similar to those used for the flight THz radiometer. The second laser did not use a dithered frequency stabilization and was considered to have better THz spectral purity. The reference laser was tuned 1–2 MHz from line center and the output of the mixer was observed with a spectrum analyzer. The combined width was less than 100 kHz. Then various amplitudes and phases of reflected power were included with no discernible effect.

Figure 15 shows the output power of the laser measured as part of thermal vacuum tests at Coherent in March 2001. The variation with temperature is mostly due to expected change in THz gain although pump power also decreases with increasing temperature to a lesser extent. Additional points in the figure prior to 2004 are from vacuum tests made at JPL or at Northrop Grumman Space Technologies, the spacecraft contractor. There are also two points

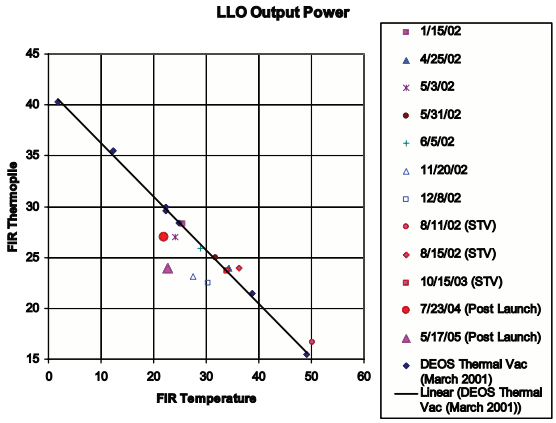

Fig. 15. GLLO output power versus temperature.

taken after launch that are separated by nearly 10 months.

The Aura spacecraft was launched on July 15, 2004, and the GLLO was first ignited in space on July 22, 2004. The GLLO has been continuously operating since then with virtually no ground intervention. Figure 16 shows a one-day sample of the temperature of the GLLO and the behavior of the pump laser output coupler. The temperature variations are due to variation in the albedo of the Earth as the spacecraft passes over it. There are 14.5 orbits per day. At the temperature extremes, the PZT reaches 0.9 or 0.1 of full range and autonomously reacquires the lock. The reacquisition time is 40 s. The temperature extremes are not usually as large and on many days no reacquisitions are required.

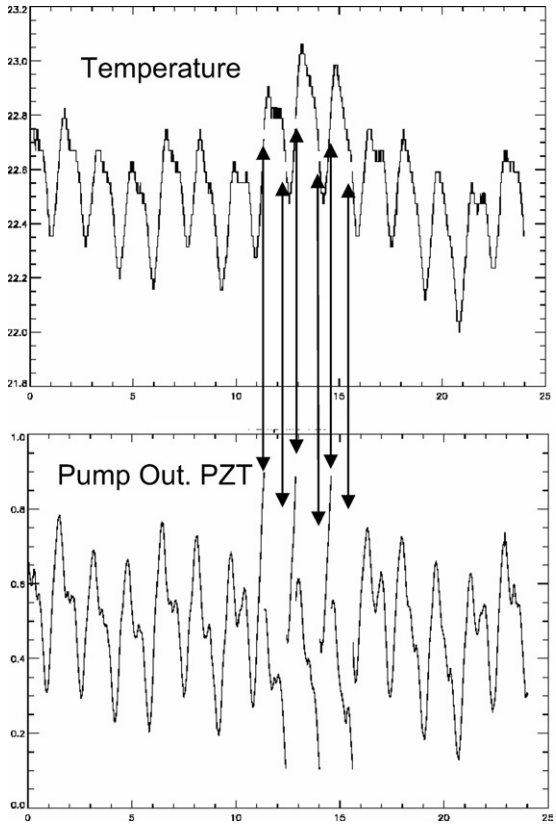

Fig. 16. GLLO re-lock behavior on-orbit.

The method used for on-orbit measure of system performance is to track the mixer bias voltage since this voltage is approximately proportional to GLLO power delivered to the mixer, assuming no degradation in the mixer. Examination of the trend shows that this signal has decreased by 18% over 30 months in orbit, indicating an 18% upper limit on the degradation observed since launch.

10. Conclusions

The GLLO utilizes high-reliability laser technology to meet the needs of the MLS measurements of OH. There was substantial performance margin at delivery and thorough modeling for the entire GLLO, including control electronics. At the time of launch, >3 years of lifetime data for the GLLO FM was accumulated. Since launch the GLLO has worked as specified for more than 30 months of operation in space.

The results of the GLLO program have shown that THz feedback effects can be mitigated successfully through the use of a "coupled-cavity" control architecture. In addition, with proper engineering care, a THz laser can be autonomously operated in a sealed-off mode in a space environment for extended periods of time.

The authors wish to acknowledge the vital contributions of the network of suppliers, and of the other team members, to this work. Research at the Jet Propulsion Laboratory, California Institute of Technology, is performed under contract with the National Aeronautics and Space Administration.

References

1. M. C. Gaidis, H. M. Pickett, C. D. Smith, S. C. Martin, R. P. Smith, and P. H. Siegel, "A 2.5 THz receiver front end for spaceborne applications," IEEE Trans. Microwave Theory Tech. **48,** 733–739 (2000).
2. E. R. Mueller, W. E. Robotham, Jr., R. P. Meisner, R. A. Hart, J. Kennedy, and L. A. Newman, "2.5 THz laser local oscillator for the EOS Chem 1 satellite," in *Proceedings of the Ninth International Symposium on Space Terahertz Technology* (NASA/JPL, 1998), pp. 563–574.
3. J. W. Waters, L. Froidevaux, R. S. Harwood, R. F. Jarnot, H. M. Pickett, W. G. Read, P. H. Siegel, R. E. Cofield, M. J. Filipiak, D. A. Flower, J. R. Holden, G. K. Lau, N. J. Livesey, G. L. Manney, H. C. Pumphrey, M. L. Santee, D. L. Wu, D. T. Cuddy, R. R. Lay, M. S. Loo, V. S. Perun, M. J. Schwartz, P. C. Stek, R. P. Thurstans, M. A. Boyles, K. M. Chandra, M. C. Chavez, G.-S. Chen, B. V. Chudasama, R. Dodge, R. A. Fuller, M. A. Girard, J. H. Jiang, Y. Jiang, B. W. Knosp, R. C. LaBelle, J. C. Lam, K. A. Lee, D. Miller, J. E. Oswald, N. C. Patel, D. M. Pukala, O. Quintero, D. M. Scaff, W. Van Snyder, M. C. Tope, P. A. Wagner, and M. J. Walch, "The Earth observing system microwave limb sounder (EOS MLS) on the Aura satellite," IEEE Trans. Geosci. Remote Sens. **44,** 1075–1092 (2006).
4. H. M. Pickett, "Microwave Limb Sounder THz module on Aura," IEEE Trans. Geosci. Remote Sens. **44,** 1122–1130 (2006).
5. W. W. Rigrod, "Homogeneously broadened CW lasers with uniform distributed loss," IEEE J. Quantum Electron. **14,** 377–381 (1978).

6. G. Busse, E. Basel, and A. Pfaller, "Application of the opto-acoustic effect to the operation of optically pumped far-infrared gas-lasers," Appl. Phys. **12,** 387–389 (1977).
7. C. R. Pidgeon, W. J. Firth, P. A. Wood, A. Vass, and B. W. Davis, "Two-photon light shift and Autler-Townes splitting in optically-pumped FIR lasers," Int. J. Infrared Millim. Waves **2,** 207–214 (1981).
8. S. T. Shanahan and N. R. Heckenberg, "Heterodyne measurement of the absolute two photon light shift in an optically pumped laser operating at 889 μm," Opt. Commun. **50,** 393–396 (1984).
9. S. H. Autler and C. H. Townes, "Stark effect in rapidly varying fields," Phys. Rev. **100,** 703–722 (1955).
10. P. M. Plainchamp, "Frequency instability measurements of the CH_3OH optically pumped laser at 70.5 and 118 μm," IEEE J. Quantum Electron. **15,** 860–864 (1979).
11. J. Heppner, C. Weiss, U. Hubner, and G. Schinn, "Gain in cw laser pumped FIR laser gases," IEEE J. Quantum Electron. **16,** 392–402 (1980).
12. A. Harth, "Pump beam propagation in circular waveguides of optically pumped far-infrared lasers," Int. J. Infrared Millim. Waves **12,** 221–237 (1991).
13. J.-M. Lourtioz and R. Adde, "Diagnostic experiments and modeling of the 118 μm CH_3OH laser," J. Physique **41,** 251–358 (1980).
14. J. H. Lee, C. L. Rettig, N. C. Luhmann, Jr., and W. A. Peebles, "Development of a far-infrared ring laser for plasma diagnostic applications," Rev. Sci. Instrum. **63,** 4678–4681 (1992).
15. R. Densing, A. Erstling, M. Gogolewski, H.-P. Gemund, G. Lunderhausen, and A. Gatesman, "Effective far infrared laser operation with mesh couplers," Infrared Phys. **33,** 219–226 (1992).